Transmission of light through sub-wavelength metallic slits

Internship project report, June-September 2006

Sanli Faez

Quantum Optics & Quantum Information, Huygens Laboratory, Niels Bohrweg 2, 2333 CA Leiden, The Netherlands
Complex Photonic Systems, University of Twente, P.O. Box 217, 7500 AE Enschede, The Netherlands

E-mail: faez@molphys.leidenuniv.nl

Abstract.

Polarization dependence of light transmission through sub-wavelength metal slits has been studied by means of near field imaging of the plane wave transmission through circular ring-slits with sub-wavelength width. The structures are engraved by focused ion beam milling through a thin layer of gold deposited on a glass substrate. Intensity and polarization of the transmitted light along the slit structures is measured simultaneously, providing enough information about dependencies on relative angle between polarization direction and local extension of the slit. Need for serial measurements at different sample orientations is avoided in this system. Our results contradict the theoretical models for single sub-wavelength slits, which predict a cut-off width of half the wavelength for TE mode transmission. In some of the analyzed structures, with a width as small as a quarter of wavelength, we have found a transmission of the TE mode that is 6 times higher than that of the TM mode.

Keywords: Sub-wavelength metal slits, Polarization mapping, Radially polarized light

1. Introduction

Here I like to discuss the objectives of this project and general motivation behind this topic of research. First I will shortly define surface plasmons and refer to their role in the trend of research for miniaturization of optical devices. Then I will state the properties that makes radial polarization of light interesting for this project. After describing the project objectives I will mention the obstacles that were encountered, which is in fact the central topic of this report.

1.1. Optics beyond the diffraction limit

In the era of miniaturization, going beyond the diffraction limit of visible light has become a major obstacle for conventional optical measurements or manipulation. Because the development of bottom-up techniques and soft lithography has achieved scales smaller than hundred nanometers, the gap between optical resolution and structural details sizes become larger. Thus, many researchers are considering new methods for optical accessing of structures with details smaller than wavelength of visible light. People think that using 'Surface Plasmons' (SPs) may be a resolution [1]. SPs are electromagnetic waves that propagate along the interface of a conductor and a dielectric. The reason SP modes can achieve high wave-vectors at visible frequencies is because they are mediated by electrons rather than free space optical fields. In fact, SPs are electron oscillations at optical frequencies which are localized at the interface of a material with a positive dielectric constant (ϵ_1) and a metal of a negative dielectric constant (ϵ_2). The dispersion relation for these surface modes is as follows,

$$k = \frac{\omega}{c}\sqrt{\frac{\epsilon_1\epsilon_2}{\epsilon_1+\epsilon_2}}. \tag{1}$$

Because the sum of dielectrics of opposite sign is in the denominator, very large wave-vectors, and thus short wavelengths, are possible at optical frequencies. Note, however, that in this argument damping is neglected. For frequencies where $k \gg \omega/c$, the damping is very large.

Beside pushing the microscopy resolution limit, SPs have the potential to be useful for new functionalities such as photonic circuits, data storage, efficient light generation and bio-photonics. It is very important to note that SPs carry also major shortcomings. Their propagation is very sensitive to surface roughness and the propagation length is restricted to finite values, roughly 40 μm for gold at excitation wavelength of 800 nm [2]. Although it is rather an old subject, surface plasmons still attract the attention of many research groups in physics, bio-physics and and micro-electronics.

1.2. Radial and azimuthal polarization of light

If the polarization of a optical polarized beam is modulated in a specific way around the propagation axis, azimuthally varying polarization with different orders of periodicity

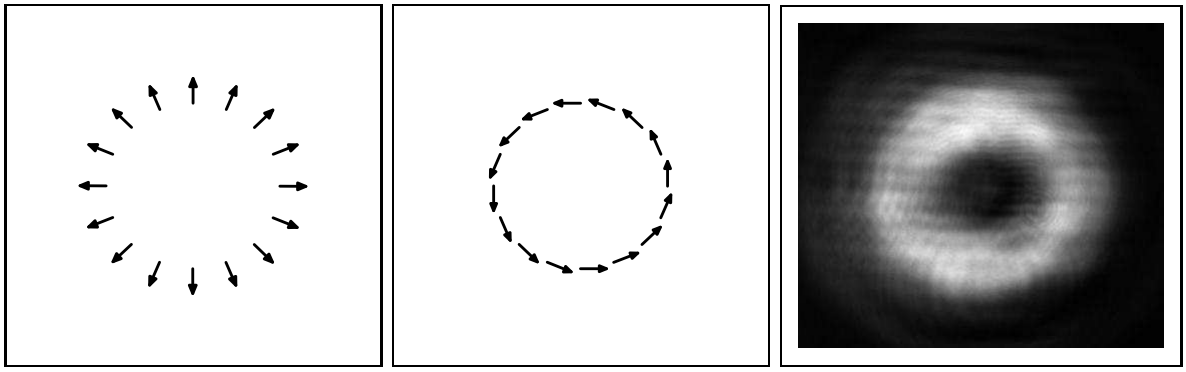

Figure 1. polarization map of *left*: radially and *center*: azimuthally polarized beam. *right*: Intensity profile of such a beam incident on a CCD camera. The donut shape is due to destructive interference at the central axis.

can be generated. Special cases with axial symmetry are radially and azimuthally polarized light (Figure 1). Recently, radially polarized beams have drawn much attention from researchers. These kind of beams differ significantly from linearly polarized beams. For example, it has been shown that they can be focused to a narrower spot, with a rotationally symmetric field distribution [3]. Due to their donut shape of focus they are supposed to have new applications for example in optical tweezers. When focusing with a high numerical aperture, the radially polarized input field leads to a strong longitudinal electric field component near the focus. In contrast, the azimuthally polarized field generates a strong longitudinal magnetic field on the optical axis, while the electric field is purely transverse and zero at the center [4]. The longitudinal component of electric field may be specially interesting when illuminating metal surfaces because, contrary to the transverse electric field, it is not nulled by the motion of free charge carriers.

Commercial devices based on liquid crystals are now available for structuring light polarization into radial or azimuthal modes in a wide range of the visible spectrum [5]. I have also used one of these devices. A short description of its working principles is presented in the experiment section.

1.3. Project objectives

Most of the experiments on surface plasmon generation on metallic surfaces are done with linearly polarized light. Corrugated surfaces and gratings are frequently used in order to enhance the coupling of incident light with SPs [6], showing frequency dependent behavior, which in turn is usually used to prove the significance of surface plasmon generation in the observed phenomena. Based on the experience on SP assisted transmission of light through sub-wavelength metal slits [7] and seeking new applications of spatial polarization convertors, this project was defined to explore the response of SP additive effects to spatially structured polarization of input beam. In other words, is it possible to induce constructive or destructive interference of SPs propagating from multiple directions toward one point? If yes, how strong is this effect. As a well-

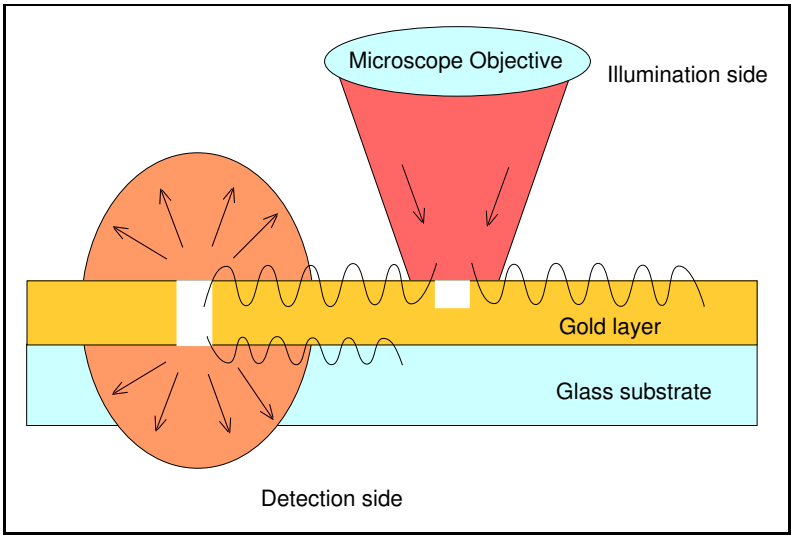

Figure 2. When light is sharply focused (NA = 0.69) on a ridge engraved in a layer of gold, some part of the SPs generated at the ridge, travel to the slit, nearby, and partially decouple to light which can be detected from the other side, after transmission through the slit.

defined reasonably well-studied spatially structured polarization, radial polarization was an attractive option. Coupling this cylindrically symmetric mode with circular ridges and/or circular slits on metallic thin layers, it was foreseen that an Airy disc equivalent in 2D surface plasmonic ground may show up, due to in phase interference of SPs which are coherently generated around the slit. Structures were designed with the idea of generating a point source for radially propagating SPs, a 2D equivalent of spherical radiation from point sources.

Having no experience with polarization variant incident beam, we decided to first perform a careful characterization of the optical response of the fabricated structures using linearly polarized. At first the light was sharply focused on part of a ridge engraved for enhancement of light coupling to SPs. A narrow slit is placed nearby and parallel to the ridge at a distance of 15 μm, which is further than the focus size but within the range of SP propagation length (Figure 2). Having propagated from the ridge toward the slit, the SPs partly convert into other SP propagation modes, and partly couple to light, mainly by scattering off the sides of the slit. The locally generated light passes through the slit and diffracts from the other side of the thin metal film. This effect is observed in the samples, but there are some observations about the polarization of outgoing light, that are contradictory to our expectation. In order to further investigate this phenomenon, I made the setup even simpler enabling the measurement of the transmission of plane wave through the slit and study its polarization dependence. There was yet another unexpected result. It is well-known, theoretically, that linearly polarized light with its electric field parallel to the long axis of the slit (TE mode) should have very low transmission through a metallic slit narrower than half the wavelength, while the TM mode transmission stays finite. I observed that in our gold samples

it is not the case. The transmission of both TE and TM modes through the slit is comparable, even when the slit width is only $\frac{\lambda}{8}$. It is very important to understand these observations, which are contrary to the theory, before taking firm steps forward in understanding plasmonic behavior in realistic metallic nano-structures. Here I report about the encountered situation and its anomaly.

1.4. Outline of this report

After the brief introduction to the project objective, I will proceed with briefly reviewing the proposed models for transmission through sub-wavelength slits in section 2 were I also bring the mathematical formulation needed for analyzing the captured data. In section 3, I will represent the setup, which was assembled for pursuing the experiments. A set of structures were fabricated on a thin film of gold supported by a glass substrate, specifically for the objectives of this projects. The fabrication and characterization of this samples will be presented in section 4. In section 5, I will present the results of the experiments and their analysis. The report will end by giving a conclusion and discussion on the conducted work in section 6 together with suggesting some possibilities for future exploration.

2. Theoretical aspects

In the first part of this section I will review briefly the available literature on transmission through slits with a width comparable to the wavelength. This theory will be later compared with the obtained results of experiments. In the second part I will describe the formulation of the method which is used to measure the polarization map of transmitted light through circular slits.

2.1. Sub-wavelength slits

The analysis of light transmission through a metal slit with a sub-wavelength width dates back to experiments done by Fizeau [8] and Lord Rayleigh (reference from [11]) who did measurements on scratches in silver mirrors. More careful theoretical and experimental investigations have later been reported [9] with more precise analysis of dielectric constant and conductivity at the slit borders and depth of the slit. The general result of these investigations was that for the metal slits wider than a wavelength, the TE mode (electric field parallel to the slit extension) should transmit more than the TM mode, but there is a cut-off for TE transmission at $w = \frac{\lambda}{2}$ where w is the width of the slit, while the TM mode transmission is still present in narrower slits. This effect is used in fabrication of polarizer filters which are based on dichroism. Quite recently it has been shown that the cut-off width in a real metal is more close to $w = \frac{\lambda}{4}$ [11]. Another recent observation shows that transmission through metallic sub-wavelength apertures can be larger than the prediction of classical aperture theory [6], which attracted a new wave of attention to the subject. The descriptions for this effect consider surface plasmon

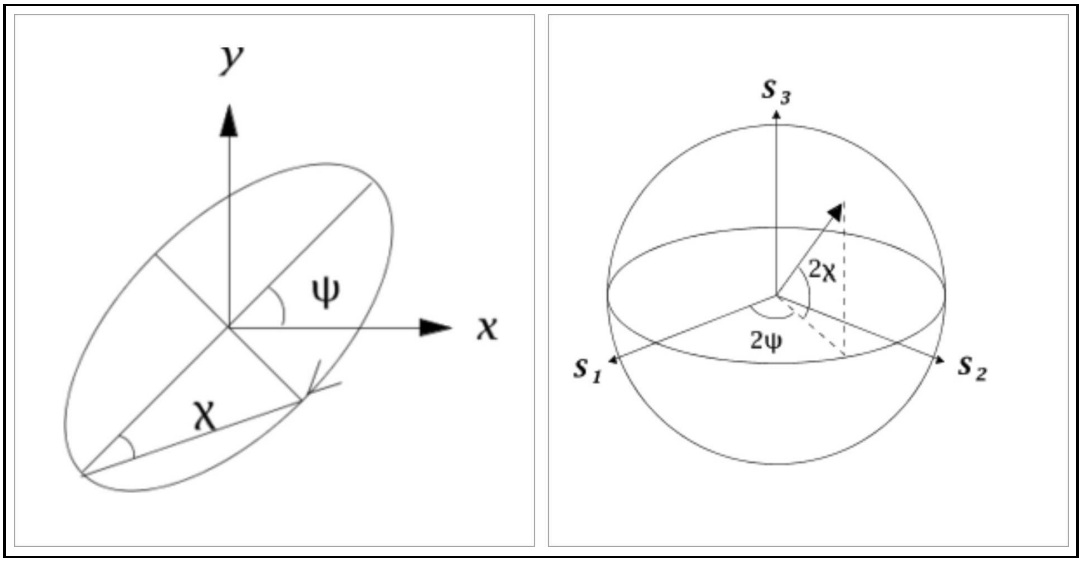

Figure 3. *left:* Visualization of a polarization ellipse, *right:* Geometrical representation of Poincarè sphere with the Stokes parameters as axes of the coordinate system.

assistance [6], coupling to waveguide modes [10], or optical phase singularities [11] as responsible for this enhancement. Resonances [11, 12] and step-wise [13] transmission have been observed experimentally and described theoretically using a variety of models. Imperfections of slit boundaries, fabrication effects on local refractive indices and surface effects makes it hard to prove or disprove one theory and keeps the discussion on this topic in full swing.

2.2. Polarimetry by measuring Stokes parameters

The Stokes parameters are a set of values that can be used to describe the polarization state of light. They were introduced by George Gabriel Stokes in 1852, as a mathematically convenient alternative to the more common description of partially polarized radiation in terms of its total intensity (I), (fractional) degree of polarization (p), and the shape of the polarization ellipse, which by itself is described by three parameters; azimuth angle (ψ), ellipticity (χ) and handedness (h) (Figure 3). Let's assume, for a general case of elliptically polarized beam, the ellipse that the tip of electrical field vector sweeps the plane which is orthogonal to propagation direction. Here, ψ is the angle between major axis of this ellipse and x-axis, χ is the arctangent of the ratio of major and minor axis of the ellipse, and h defines the direction of rotation of the electric field which can be ± 1. On the other hand, the electric field vector can also be described by two complex numbers, which oscillate with equal frequencies and their real parts give us the Cartesian components of electric field in a plane perpendicular to the direction of propagation. In other words, for a coherent plane wave propagating in the z direction, the electric field can be fully described by

$$\vec{\mathbf{E}}(\mathbf{r},t) = \mathbf{Re}[(E_1\hat{\mathbf{x}} + E_2\hat{\mathbf{y}})e^{-ikz+i\omega t}], \tag{2}$$

where E_1 and E_2 are complex numbers. In this case the Stokes parameters are defined as

$$\begin{aligned} S_0 &= E_1E_1^* + E_2E_2^*, \\ S_1 &= E_1E_1^* - E_2E_2^*, \\ S_2 &= E_1E_2^* + E_1^*E_2, \\ S_3 &= -i(E_1E_2^* - E_1^*E_2). \end{aligned} \tag{3}$$

If we construct a vector in polar coordinates with a length equal to the total intensity of light times its degree of polarization, and with azimuth and altitude of 2ψ and 2χ, the Stokes parameters, (S_1, S_2, S_3), are the components of this vector in Cartesian coordinates. S_0 is just the total intensity of light including both the coherent and incoherent parts. For fully polarized beams, the following relations give the ellipticity parameters:

$$\begin{aligned} \tan 2\psi &= \tfrac{S_2}{S_1}, \\ \sin 2\chi &= \tfrac{S_3}{S_0}, \\ h &= \mathrm{sgn}(S_3). \end{aligned} \tag{4}$$

With suitable polarization filters, it is possible to obtain the Stokes parameters of a coherent beam by at least four intensity measurements. For a partially polarized beam, an additional measurement is needed to obtain S_0, giving the degree of polarization when comparing with $\sqrt{S_1^2 + S_2^2 + S_3^2}$. These four measurements are, 1- transmitted intensity from a horizontal polarizer (I_0), 2- transmitted intensity from a vertical polarizer (I_{90}), 3- transmitted intensity from a polarizer at 45 degrees to horizontal axis (I_{45}), 4- intensity after passing a quarter waveplate followed by a polarizer at 45 degrees to the fast axis of the waveplate. To avoid an error in determination of S_2, I measured another intensity which is the transmitted intensity from a polarizer at -45 degrees to horizontal axis (I_{-45}). In the results shown in this paper I was only interested in the azimuth angle, *i.e.* 2ϕ . For this parameter, only S_1 and S_2 are needed which can be derived from three or four measurements using the following relations:

$$\begin{aligned} S_1 &= I_0 - I_{90}, \\ S_2 &= 2I_{45} - (I_0 + I_{90}) = I_{45} - I_{-45}. \end{aligned} \tag{5}$$

3. Experimental aspects

In this section I will first describe the setup used for the measurements. The designed sample and its way of fabrication and characterization will follow afterwards.

3.1. The setup

The setup designed for this experiment (Figure 4) is meant to enable two kind of measurements. The first purpose is to capture the near-field image of the diffracted light through the slit structures. The second purpose is to measure the amount of second harmonic generation in reflection at normal incidence. I will not present the results of

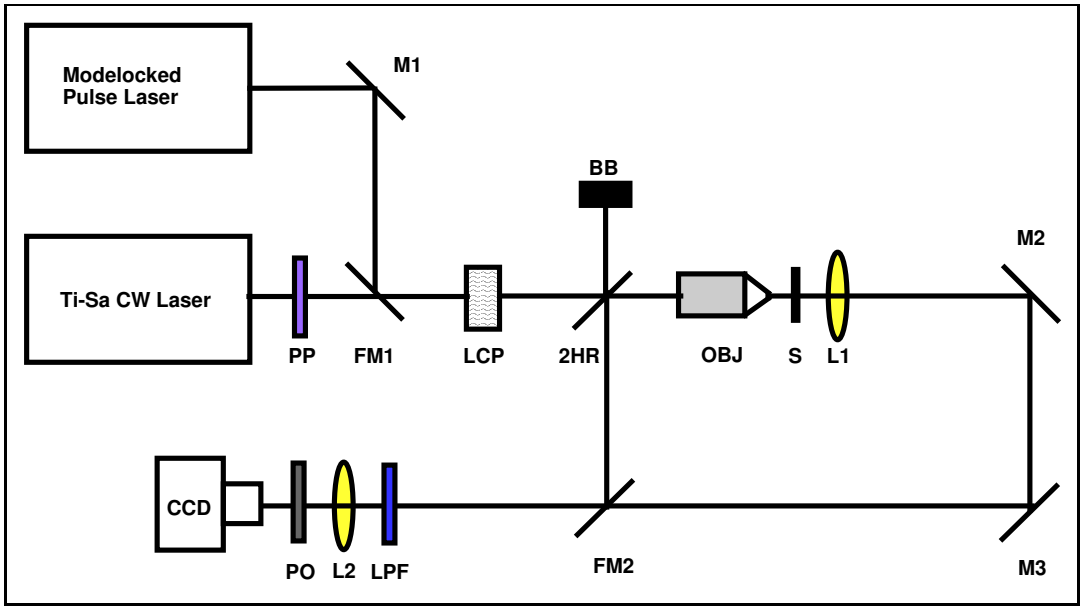

Figure 4. Schematic view of the experimental setup. M1: silver mirror, FM1: flipping silver mirror, LCP: radial/azimuthal polarizer, PP: $\lambda/2$ or $\lambda/4$ phase plate, 2HR: second harmonic remover, BB: beam blocker, OBJ: microscope objective (0.49 NA) on translation stage, S: sample on translation stage, L1: focusing lens (f =16 mm) on translation stage, M2 and M3: near infrared mirrors, FM2: flipping coated mirror for λ =400 nm, LPF: removable UV-transmitting filter (BG39), L2: removable focusing lens (f =50 mm), PO: adjustable polaroid filter

the latter experiment in this report. For each purpose a different light source is used. A CW Ti-Sapphire laser tunable over the spectral range of 740-830 nm, optically pumped by 3 W green laser (Spectra Physics, Millenia), is used for transmission measurements. The polarization of the output light can be rotated by a $\frac{\lambda}{2}$ phase plate or made circular by a $\frac{\lambda}{4}$ phase plate. For second-harmonic generation measurement a mode-locked pulse laser (Coherent, Vitesse) was used that makes pulses of 70 fs duration (FWHM) with its central frequency at 800 nm and average power of 116 mW. This laser is optically pumped by a 10 W green laser beam (Coherent, Verdi). The polarization of pulses is parallel to the optical table. Switching between the two light sources is possible using a flipping mirror without interfering with the alignment of other parts of the setup.

The laser beam is passed through a radial-azimuthal polarization converter (Arcoptix) that contains a nematic liquid crystal [5]. I'll shortly describe the working principles of this device at the end of this section. The beam then passes a special mirror (Laser Components, HR400/45) which is needed for second-harmonic reflection measurements and can be removed for transmission experiment. This mirror is transparent ($> 90\%$) at 800 nm but highly reflective ($> 99\%$) for incident light of 400 nm wavelength at 45 degrees of incident angle. Due to slight polarization dependence of transmission, the beam intensity around its axis gets distorted. A high NA microscope objective focuses the beam into a spot of 3 micron diameter on the sample. High values of NA are specially needed for the second-harmonic generation experiment. The objective

and the sample are both mounted on stages with 3 translational and 2 rotational degrees of freedom so that they can be aligned easily and with high accuracy. The translation stage for the sample has a precision of 1 micron, which can be used for finding the structures written into the gold layer. Once the structure is in the field of view of the lens, optimal adjustments are done by maximizing the transmission trough the slits. Fortunately, direct transmission through bulk gold is also detectable for the CCD camera; this property can be used to measure, in the near-field images, the distance from the center of focus of the incident beam to the structures.

The near-field image of diffracted light from the sample is on the CCD screen. I use a lens with a high NA (~ 0.6) in order to collect as much light as possible. The CCD is put far from the lens in order to achieve high magnification (~ 200 times). Two near-infrared mirrors reflect the light in order to enable me to fit the setup in a smaller area on the optical table. A polarizer filter, quarter wavelength phase plate, and necessary attenuation filters can be placed in front of CCD camera whenever needed. In the second-harmonic generation experiments, the transmission channel can be used for adjusting the sample position.

The reflected light from the sample is gathered by the same microscope objective. A high fraction of the generated second-harmonic light is guided by two mirrors and focused on the CCD by a lens. The fundamental reflection is highly attenuated (by a factor of 10^{-12}) by low reflection of mirrors and a 3 mm thick UV-transmitting glass filter (Schott BG39). The CCD camera (Apogee Alta U1) has an array size of 768×512 pixels and pixel size of 9×9 microns, and is controlled by a PC. The detector can be cooled down to 243 K, which might be useful for second-harmonic detection. Due to sufficiently high power of the incident beam, in all of the transmission experiments, a very good signal to noise ratio (> 100) can easily be achieved.

3.2. About the radial-azimuthal polarization converter (LCP)

The radial-azimuthal polarization converter is a nematic liquid crystal (LC) cell which spatially structures the polarization of a collimated linearly polarized beam. The cell has one uniform and one circularly rubbed alignment layer. The local alignment of the LC in the polarization converter is that of a twisted cell, with a twist angle given by the local alignment layers. Azimuthally or radially polarized output is generated when the incident beam polarization is parallel or perpendicular to the uniform alignment layer. Each of the two polarizations can be selected by an extra liquid crystal layer, which can rotate the incident polarization by 90 degrees. A defect line arises at the border of clockwise and counter-clockwise rotation of polarization, the upper and the lower part (Figure 5). Therefore, a half-wavelength retardation is needed for one of the two parts in order to correct the phase mismatch, which is done by a tunable half-wave LC phase plate included in the device. This device should be tuned properly for each wavelength but can be used for a spectral range of 400-1700 nm.

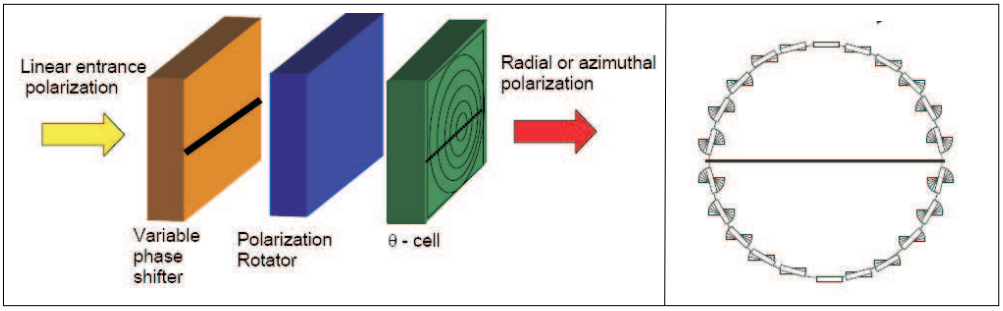

Figure 5. *left:* 3 liquid crystal cells incorporated in Arcoptix radial-azimuthal polarization converter *right:* Liquid crystal alignment in the polarization converter for a stable configuration. The line in the center represents a defect line present because of different twist sense of the upper and lower part. This defect is corrected by tuning the variable phase shifter to induce half a period phase retardation in one part.

4. Sample

In this section I will describe the process of sample preparation and characterization. A short overview of Focused Ion Beam milling is also brought to the readers attention.

4.1. Sample preparation

The sample consists of structures engraved in a thin layer of gold deposited on a glass substrate. For this sample, first, 10 nm of Titanium is deposited on an optically flat glass substrate, which plays the role of adhesion layer. Later, 200 nm of gold is sputtered over the Titanium layer. Desired slit and ridge structures are then engraved by Focused Ion Beam milling. The sample is then very gently cleaned and mounted on a holder which protects the sample from being touched. The structures consist of circular slits or ridges with different radius and width. Some of the circular structures are accompanied by a sub-wavelength hole at their center which is supposed to act as a local probe of surface plasmon concentration which couples to light by scattering from this hole. Or else the direct transmission from the hole can interfere with the plasmonic channel arising from the circular slit around. This interference appears as spectral fringes in the transmission spectrum. Details of structure dimensions are given below Figure 6.

4.1.1. about "Focused Ion Beam Milling" :

Focused ion beam milling, also known as FIB, uses a focused beam of gallium ions for surface manipulation or imaging. Gallium is chosen because it is easy to build a Gallium liquid metal ion source (GLMIS). In a GLMIS, gallium metal is placed in contact with a tungsten needle and heated. Gallium wets the tungsten, and a huge electric field (greater than 10^8 Volts per centimeter) causes ionization and field emission of the gallium atoms. These ions are then accelerated to an energy of 10-40 KeV , and then focused onto the sample by electrostatic lenses. A modern FIB can deliver tens of nanoAmps of current to a sample, or can image the sample with a spot size on the

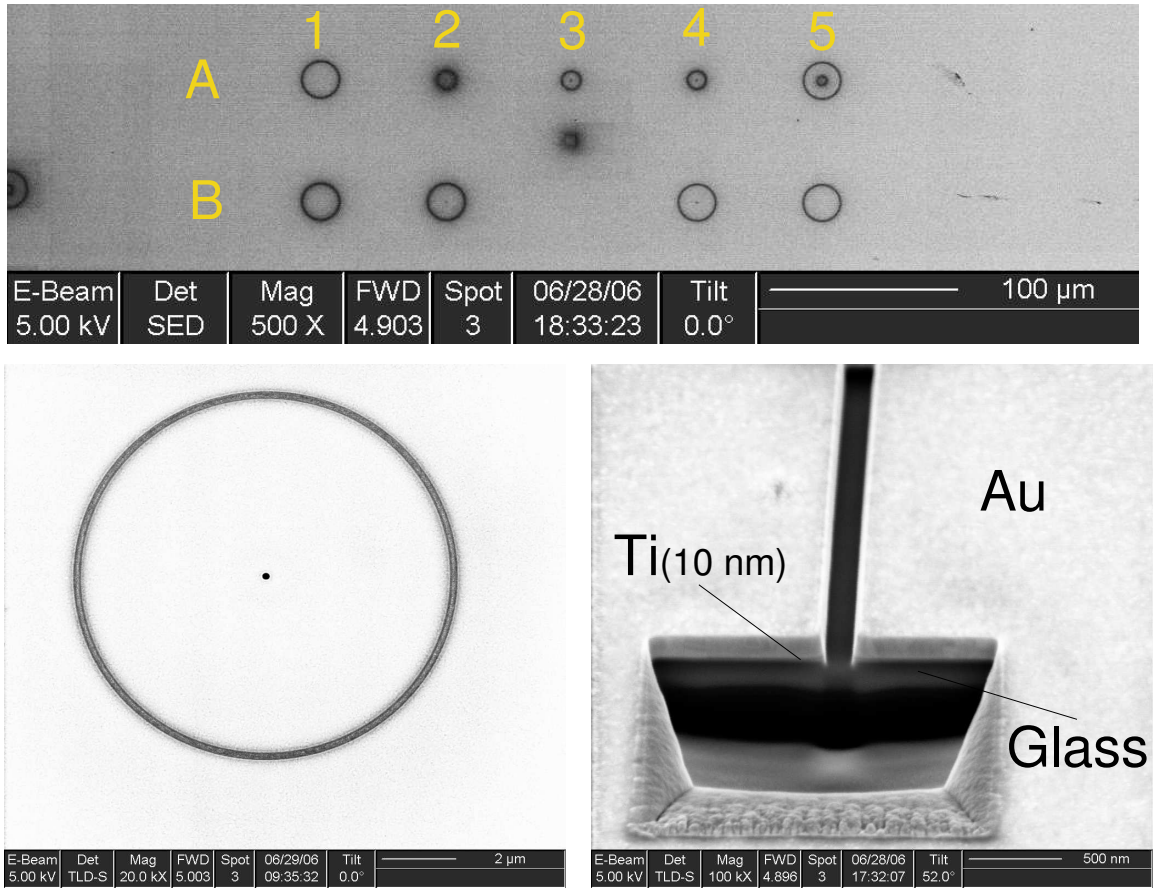

Figure 6. *Top*: Scanning electron micrograph of test structures which are milled exactly with the same conditions as optically measured structures. Here d is the diameter, w is the width and t is the depth of the structures. A1: ring-slit $d = 20\,\mu$m $w = 100$ nm $t = 200$ nm, A2: ring-slit $d = 10\,\mu$m $w = 200$ nm $t = 200$ nm plus 200 nm hole at the center, A3 and A4: ring-ridge $d = 10\,\mu$m $w = 200$ nm $t \simeq 70$ nm plus 200 nm hole at the center, A5: ring-ridge $d = 20\,\mu$m $w = 100$ nm $t \simeq 70$ nm concentric with ring-slit $d = 5\,\mu$m $w = 200$ nm $t = 200$ nm, B1: ring-slit $d = 20\,\mu$m $w = 200$ nm $t = 200$ nm, B2: ring-slit $d = 20\,\mu$m $w = 200$ nm $t = 200$ nm plus 200 nm hole at the center, B4: ring-ridge $d = 20\,\mu$m $w = 200$ nm $t \simeq 70$ nm plus 200 nm hole at the center, B4: ring-ridge $d = 20\,\mu$m $w = 200$ nm $t \simeq 70$ nm plus triangular aperture with 3 μm sides at the center. *Down-left*: A ring slit (A3 in the top image) in close up. *Down-right*: cross section of a test structure made visible after opening one side of the section by high power milling

order of a few nanometers. FIB is inherently destructive to the specimen. When the high-energy gallium ions strike the sample, they will sputter atoms from the surface. Gallium atoms will also be implanted into the top few nanometers of the surface, and the surface of crystalline materials will be made amorphous. This has been shown by imaging the cross section of Silicon wafer after FIB milling [14]. I have found no result showing any effect of FIB milling on dielectric constant at optical frequencies.

4.2. Sample characterization

Scanning electron microscope is used to quantitatively and qualitatively measure the result of fabrication process. In order to avoid the electron beam affecting the optical properties of the structures, similar test structures are made at a different position on the sample during the same fabrication session. Figure 6 shows the SEM images recorded of these test structures. The structure dimensions and shape are as expected but no more information on local optical properties of the structure like conductivity or dielectric constant can be obtained from these images.

5. Results

As mentioned in the discussion about project objectives in section 1.3, the main goal of this report is shifted toward verifying the anomalous observations, which are contrary to the theory of transmission through sub-wavelength slits. In this section I will report the transmission measurements of plane coherent waves through some of the structures and their polarization properties. For these measurements a CW laser (fixed at 780 nm) is used and some of the components are removed from the experimental setup in order to create the simplest conditions that are possible. These components include FM1, LCP, 2HR, OBJ, LPF, FM2 and L2 as introduced in Figure 4. The remaining setup, shown in Figure 7, deals with a basic measurement. A Gaussian beam of 1 mm in diameter, illuminates the selected structures of the sample at normal angle of incidence. The near-field image of the light diffracted through this single structure is imaged by L1

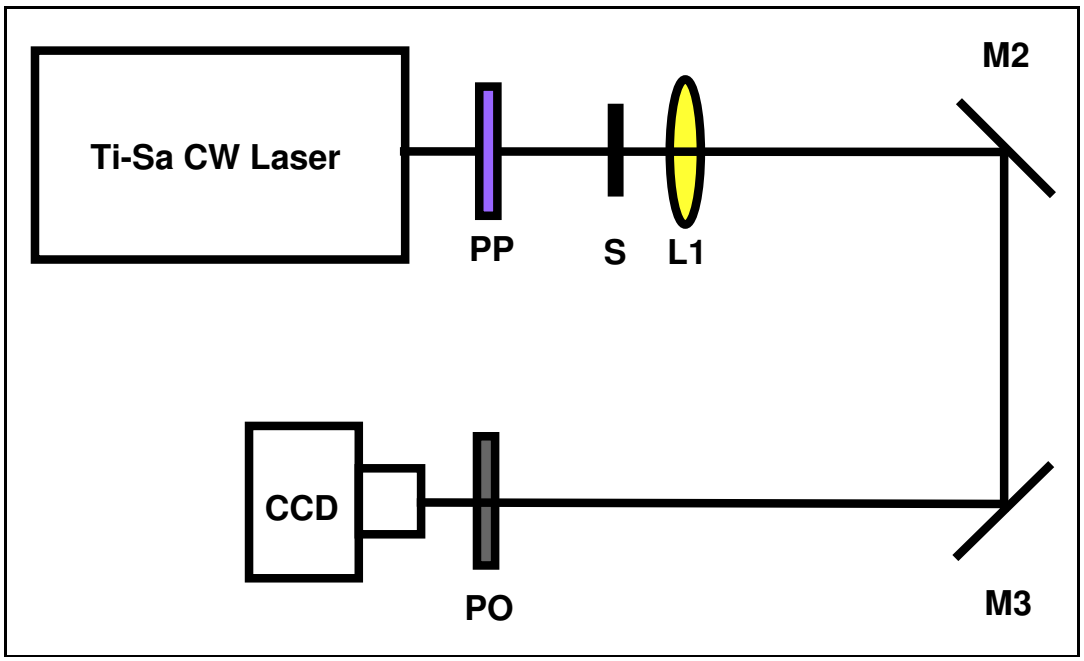

Figure 7. Schematic view of the simplified setup. PP: $\lambda/2$ or $\lambda/4$ phase plate, S: sample on translation stage, L1: focusing lens (f =16 mm) on translation stage, M2 and M3: near infrared mirrors, PO: adjustable polaroid filter

on the CCD screen with roughly 200 times magnification. Attenuation of the beam is done by putting proper neutral density filters in front of the camera in order to prevent overexposing the CCD.

In this section I will first report the measured total intensity of transmitted light from around a ring-slit for different dimensions of the structure, in section 5.1. The absolute value of transmitted light intensity is not important because relative intensities at different points of a single image are enough for comparison with the theory. In fact this is one strong point of this experiment and our sample design, because all the needed data is captured in one shot. The polarization map of transmitted light around the ring-slits are measured using the method described in section 2.2. The results of these measurements are presented in section 5.2.

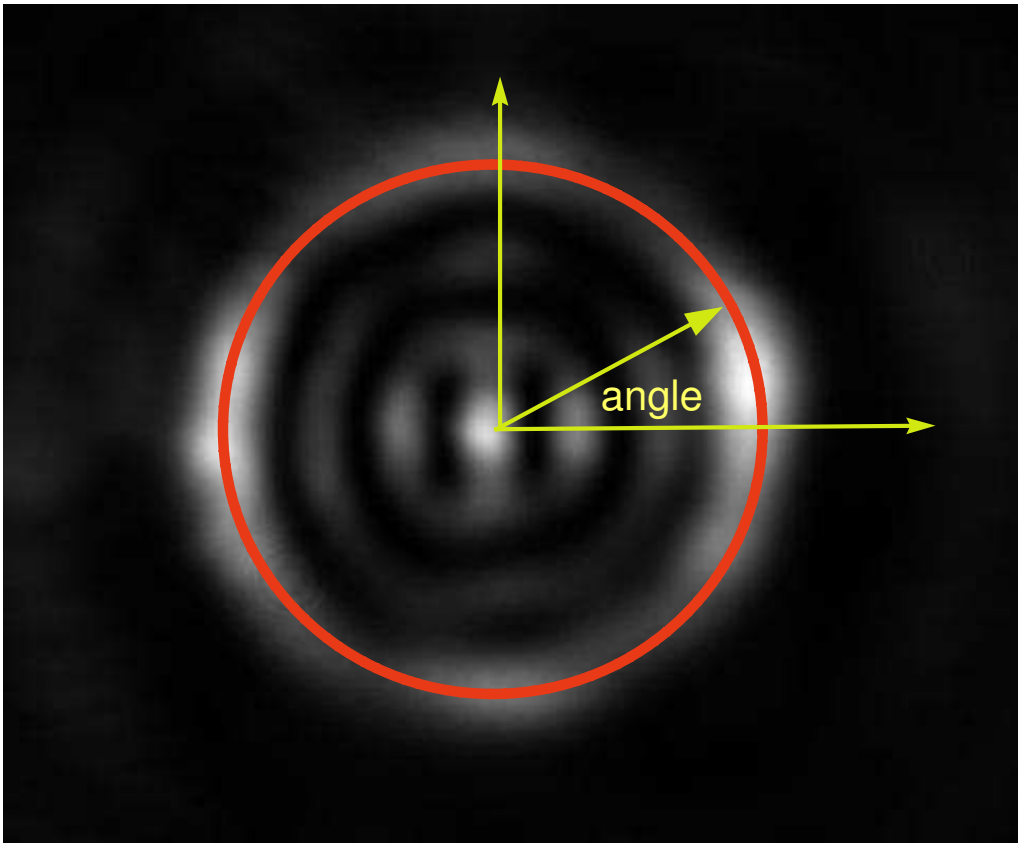

Figure 8. Near-field image of the diffraction pattern generated by a ring-slit of diameter $d = 20\,\mu$m, and width $w = 200$ nm. The structure is illuminated by a plane wave with linear polarization in the vertical direction, 90 degrees. The bright circle is the ring-slit, itself. The other patterns are, supposedly, due to diffraction from the imaging lens finite aperture. The intensity and polarization map around the slit is extracted from this picture and similar others, as described in section 2.2 and is plotted versus the angle in Figure 9 for different combination of incident polarization and structure.

5.1. Total transmission intensity

Using the simplified setup illustrated in Figure 7, near-field image of a plane wave diffraction from circular sub-wavelength slits has been captured (see Figure 8 as an example). The transmission intensity from each point of the slit is assumed to be proportional to the amount of light focused on CCD screen in these images. This intensity map is plotted versus the azimuthal angle in Figure 9. For extracting this data, first, the radius of maximum averaged intensity has been considered as the slit. For getting each data point in these graphs, a $10 * 10$ pixels neighborhood of a point on this circle is averaged. A substantial signal to noise ratio is present in all the measurements and the background is automatically subtracted by the CCD control program.

In the top frame of Figure 9 the incident light polarization is circular. The slits have a width equal to 100 nm or 200 nm, which is much less than $\frac{\lambda}{2}$. As described in chapter 2.1, it is expected that the transmission of polarization parallel to a sub-wavelength slit should be zero while the transmission of the orthogonal polarization is finite. The incident intensity all over the ring-slit is homogeneous because the beam size is much larger than the structures. In case of circular polarization the magnitude of the polarization component which is locally orthogonal to the ring circumference is supposed to be constant around the ring-slit, therefore a uniform intensity transmission around the structure is expected, which is evidently not the case in this plot. For the 100 nm wide slit the intensity is more uniform than for the slits with 200 nm width. The non-uniformity in this intensity pattern does not show wavelength dependence as I tune the emission wavelength of the laser between 750 nm to 820 nm. It has been shown that surface plasmon interference effects can modulate the intensity in the far field [7] but this effect is not enough for describing the observed intensity profile for two reasons. First reason is that the modulation due to interference is weaker than what I have observed, and secondly, the interference pattern should change as a result of varying the light frequency.

In the bottom frame of Figure 9 the incident light polarization is linear in the vertical direction (the electric field is at 90 degrees corresponding to the plotted scales). For the ring-slit of 100 nm width, the transmission is not zero at angles where polarization is parallel to the slit(at 0° and 180°), as required by the theory. The visibility of the variations of this curve in the graph may seem to be low, but this is just because the scales on the vertical axis has been taken the same as for 200 nm wide slits, so that comparison may be easier. In fact, by comparing the black squares and the red triangles, one can rapidly find out from this graph that the average transmission of the slit with the same diameter and half the width reduces to around $\frac{1}{8}$ of the average transmission from the wider slit. The anomaly in transmission pattern is even more surprising for the 200 nm wide slits which show up to 6 times more transmission of the transverse electric mode than the transverse magnetic mode, which is in full contradiction to the described available theories. This anomaly is present for all the 3 tested diameters of the ring-slits (5, 10 and 20 μm) and becomes more pronounced as

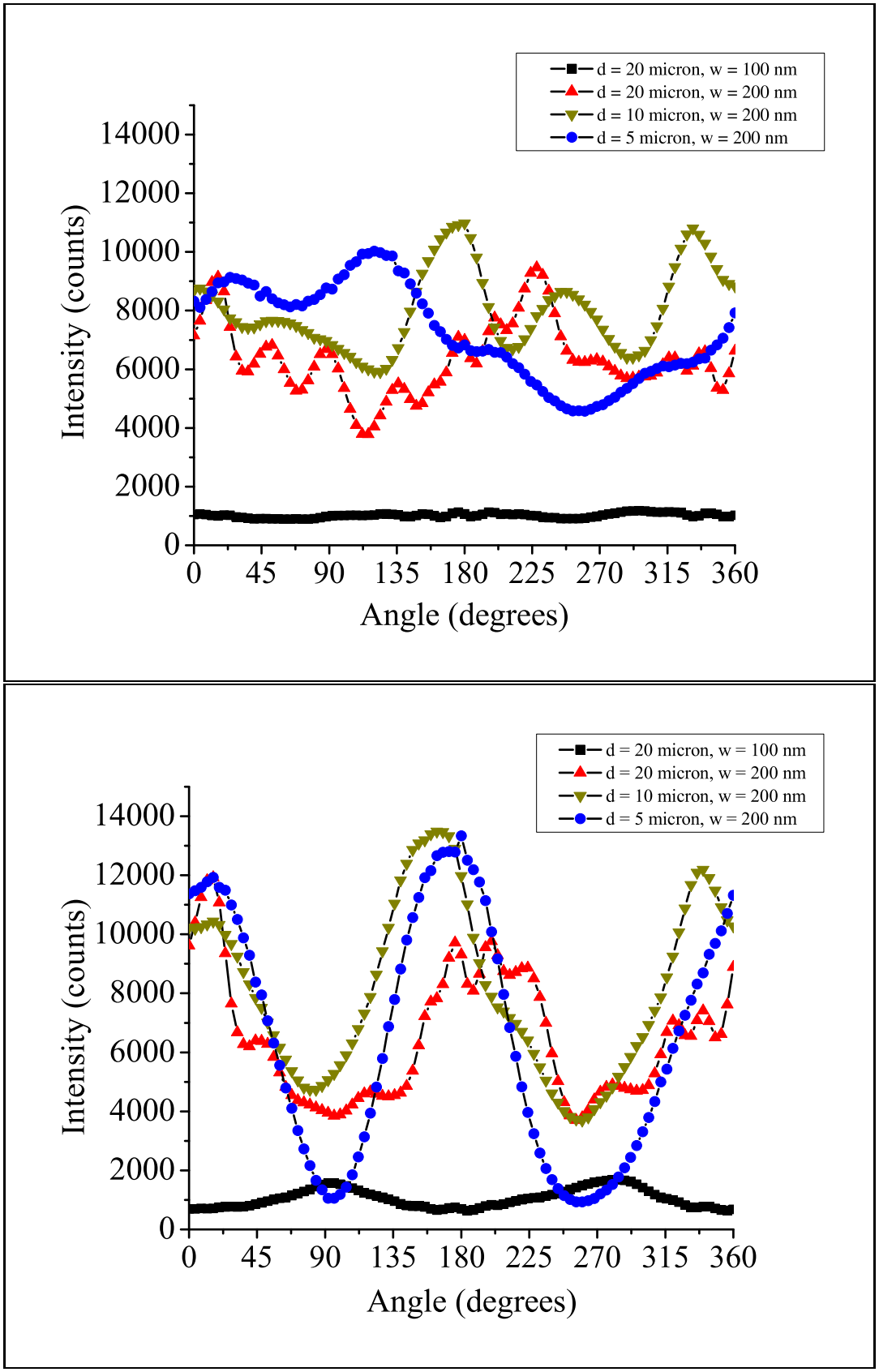

Figure 9. Transmitted intensity versus angle around the ring-slits with different diameters, d, and widths, w, for different incident polarizations (λ = 800nm); *top*: circular, *bottom*: linear and in the vertical direction (90 degrees). The exposure time is kept constant through this set of measurements.

the diameter decreases.

5.2. Polarization map

As described in 2.2, using suitable filters, one can draw the polarization map of transmitted light from the combination of 4 measurements. Figure 10 shows this polarization map for transmission of circular and linear polarization through 100 nm and 200 nm wide ring slits of 20 μm in diameter. The only map which is similar to the expected picture from theory is the transmission of circular polarization through 100 nm wide ring-slit, which shows projection of output polarization on the normal to the local direction of the slit. In the rest of these plots, forms of polarization rotation, including linear and circular birefringence and dichroism is evident which can hardly be explained based on the current available theory and experimental assumptions for the optical properties and geometrical specification of these structures. My observations

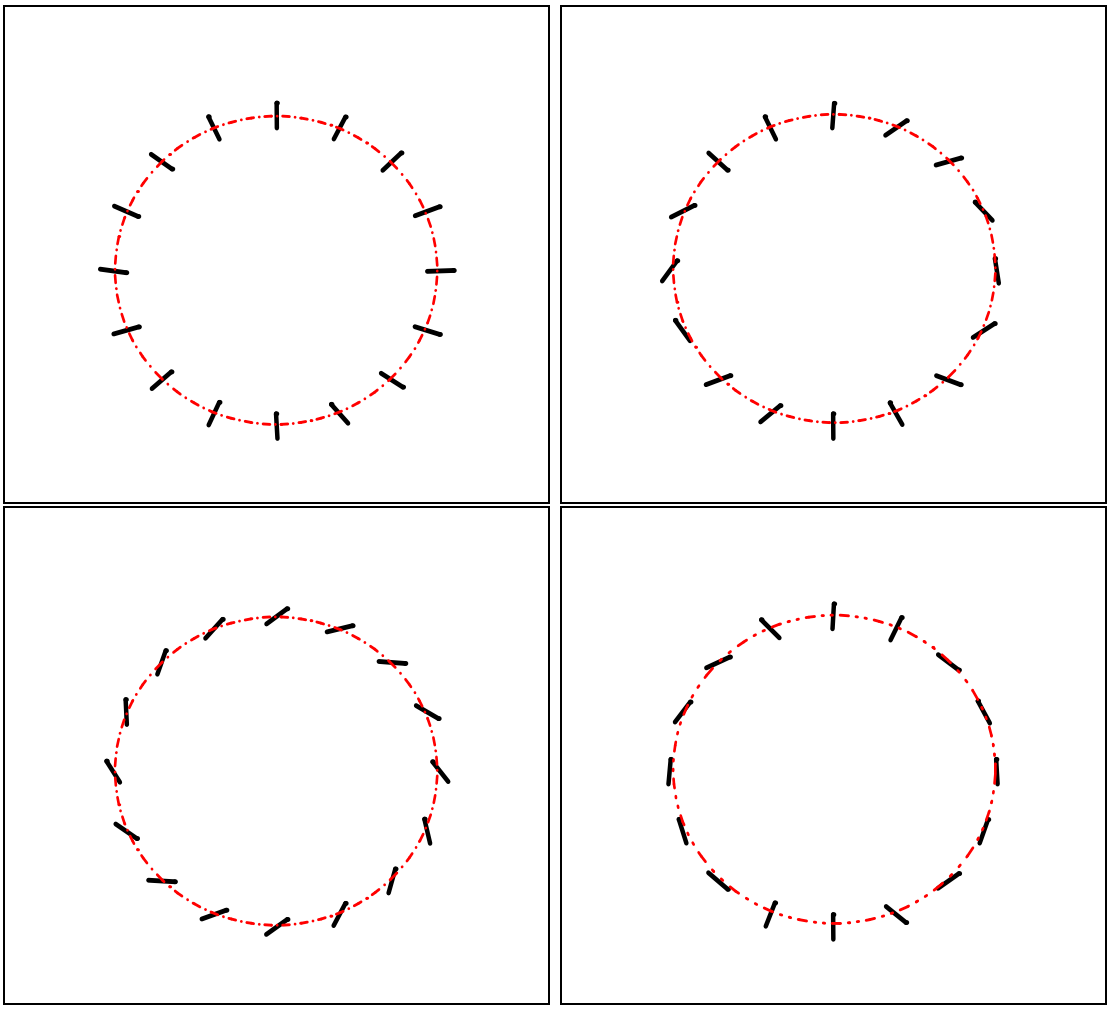

Figure 10. Polarization map around the ring-slits of 20 μm diameter with different widths; *top*: 100 nm, *down*: 200 nm, and for different input polarization; *left*: circular, *right*: linear and in the vertical direction (90 degrees)

confirm earlier unpublished results of N. Kuzmin on various samples. These results show that our structures act similar to spatial polarization modulators but in a very tiny scale. This kind of form birefringence have been previously observed and described in gratings [15]. By incorporating those observations in computer generated grating patterns, they have become a practical tool for spatially modulating polarization of light. Understanding the physics behind our observations may be helpful in engineering sub-wavelength structures that are useful for practical purposes such as micro-sensors or photonic circuits.

6. Conclusion and Discussion

An optical setup for studying both transmission properties of radially and azimuthally polarized light through sub-wavelength slits and second harmonic generation at the sharp focus of this beam has been assembled. Using this setup, second harmonic light was detected for highly focused radially polarized beam at normal incidence on gold layer of 200 nm, but was absent for azimuthal polarization. This result is in agreement with the recently reported experiment by Biss and Brown [16].

The transmission experiments resulted in observing anomalous phenomena, namely unexpected birefringence and dichroism of sub-wavelength slits, which were in contradiction with the current theories. Our specific case of slit structures provided us with the opportunity of showing this anomaly in a single near-field image of the diffraction pattern from these structures. In order to confirm these observations simpler arrangements have been used for testing transmission properties of collimated light beam with various polarizations through sub-wavelengths slits. Polarimetry of the diffracted pattern is simplified in this setup. Serious contradictions between the results of these experiments and the available theory has been shown. Interesting observations of spatial modulation of incident light polarization by our slit structures are reported that may be inspiring for fabrication of miniature, polarization-engineered light sources.

The contradiction brings up some questions about the the real material properties and structural specifications of the fabricated structures. Although the geometry of the structures is well observed in SEM pictures, it may well be that the local optical properties of gold have been changed during the fabrication process due to impinging of Gallium ions or sputtering of removed material from the points engraved in the milling process. Alternative fabrication methods, like lithographic technics or mask evaporation, or using single crystalline gold layer instead of poly-crystalline layer, may help in clarifying the real impact of fabrication process. More detailed experiments are needed to probe the local optical properties of these samples. The result of these experiments together with applying sensitivity analysis to the theory may lead to a better understanding of the optical response of sub-wavelength metal structures. Till then, the interpretation of the results of these kind of experiments should be done with great care.

Acknowledgement

This project has been done under close supervision of Dr. Eric Eliel in the Quantum Optics and Quantum Information group in Leiden University. Hereby I thank him for his careful and friendly supervision. Even after the practical job was done, Eric thought me a lot by carefully correcting my report. I also thank my supervisor in University of Twente, Dr. Allard Mosk, for his useful comments on the project proposal and of course for reading and commenting on this report. I learned a lot from Prof. Gert 't Hooft, Dr. Martin van Exter, Dr. Michiel de Dood, and Drs. Nikolay Kuzmin. The sample was made by Dr. Paul Alkemade from Delft University with the help of Nikolay. I should thank all the group members for their hospitality and I specially like to thank Daniëlle van Raaij for here compassionate cooperation in arranging the organizational issues.

References

[1] WL Barnes, A Dereus and TW Ebbesen, *Nature* **424**, 824 (2003).

[2] B Lamprecht, JR Krenn, G Schider, H Ditlbacher, M Salerno, N Felidj, A Leitner, FR Aussenegg and JC Weeber, *Appl. Phys. Lett.* **79**, 51 (2001).

[3] R Dorn, S Quabis and G Leuchs, *Phys. Rev. Lett.* **91**, 233901 (2003).

[4] DW Diehl, RW Schoonover and TD Visser, *Optics Express* **14**, 3030 (2006).

[5] M Stalder and M Schadt, *Opt. Lett.* **21**, 1948 (1996).

[6] T Thio, KM Pellerin, RA Linke, HJ Lezec and TW Ebbesen, *Opt. Lett.* **26**, 1972 (2001).

[7] HF Schouten, N Kuzmin, G Dubois, TD Visser, G Gbur, PFA Alkemade, H Blok, GW 't Hooft, D Lenstra and ER Eliel, *Phys. Rev. Lett.* **94**, 053901 (2005).

[8] MH Fizeau, *Ann. Chem. (Phys.)* **63**, 385 (1861).

[9] RV Jones and JCS Richards, *Proc. Roy. Soc. London, Series A***225**, 122 (1954).

[10] Q Cao and, P Lalanne, *Phys. Rev. Lett.* **88**, 057403 (2002).

[11] HF Schouten, TD Visser, D Lenstra and H Blok, *Phys. Rev. E* **67**, 036608 (2003).

[12] J Lindberg, K Lindfors, T Setälä, M Kaivola, and AT Friberg, *Optics Express* **12**, 634 (2004).

[13] EA Montie, BC Cosman, GW 't Hooft, MB van der Mark, and CWJ Beenakker, *Physica B* **175**, 149 (1991).

[14] S Rubanov and PR Munroe, *Journal of Microscopy*, **214**, 213 (2004).

[15] Z Bomzon, V Kleiner, and E Hasman, *Opt. Lett.* **26**, 33 (2001).

[16] D P Biss and T G Brown, *Opt. Lett.* **28**, 923 (2003).